PHYSICAL REVIEW B **91**, 241201(R) (2015)

Temperature and carrier-density dependence of electron-hole scattering in silicon investigated by optical-pump terahertz-probe spectroscopy

T. Terashige, H. Yada, Y. Matsui, T. Miyamoto, N. Kida, and H. Okamoto
Department of Advanced Materials Science, University of Tokyo, Kashiwa, Chiba 277-8561, Japan
(Received 27 January 2015; revised manuscript received 12 May 2015; published 5 June 2015)

We measured the optical conductivity $\tilde{\sigma}(\omega)$ spectra of photodoped silicon by optical-pump terahertz-probe spectroscopy and analyzed them with a two-carrier Drude model. Taking into account the values of electron (hole)-phonon scattering rates previously reported in chemically doped silicon, we evaluated the electron-hole scattering rates $\gamma_{\text{e-h}}$. From 293 to 90 K, the magnitudes and temperature dependence of $\gamma_{\text{e-h}}$ were successfully reproduced by a theoretical model including the effects of Rutherford scattering, Coulomb screening, and Pauli exclusion. This suggests that these three factors dominate electron-hole scattering processes in silicon. Below 90 K, $\gamma_{\text{e-h}}$ becomes larger than that of the theoretical curve, which is attributable to a prolongation of the relaxation time of hot carriers.

DOI: 10.1103/PhysRevB.91.241201 PACS number(s): 72.10.Di, 72.40.+w, 72.20.Dp, 78.47.jb

Carrier dynamics in electron-hole systems has been one of the central issues in the physics of semiconductors [1–7], not only for the emergence of interesting physical phenomena such as the exciton-Mott transition [1,2] and Bose-Einstein condensation of excitons [3], but also for the development of modern optoelectronic devices. In conventional inorganic semiconductors, the scattering rates of the free carriers and energy intervals of exciton levels (or exciton binding energies) fall in the terahertz frequency region. Recent developments in terahertz time-domain spectroscopy (THz-TDS) have enabled us to observe the dynamics of photogenerated carriers and/or excitons. For example, in silicon, the exciton binding energy and energy splitting between $1s$ and $2p$ excitons are 14.7 meV ($\sim$3.5 THz) and 10 meV ($\sim$2.4 THz), respectively, so that induced absorption due to excitons as well as Drude-type responses of photogenerated carriers can be directly detected by a combination of the pump-probe (PP) method and THz-TDS [3,6,7]. Using such an approach, the exciton-Mott transition has been indeed demonstrated [3,4].

When we consider applications of semiconductors to optoelectronic devices, it is significant to elucidate the scattering mechanisms of photocarriers. A mobility of carriers is determined by a scattering rate γ via the simple equation $\mu = e/m^*\gamma$, where m^* and e are an effective mass and the elementary charge, respectively. For chemically doped carriers, scatterings are known to consist of two processes: carrier-phonon scatterings and carrier-ionized-impurity scatterings [8]. On the other hand, for photocarriers, electron-hole scatterings would play significant roles in addition to carrier-phonon scatterings [9–13]. However, experimental studies clarifying the mechanism of electron-hole scatterings are lacking.

In the present study, in order to clarify the mechanisms of electron-hole scattering in semiconductors, we applied optical-pump terahertz-probe spectroscopy on silicon, which is a typical indirect-gap semiconductor [Fig. 1(a)] [14], and determined its complex optical conductivity $\tilde{\sigma}(\omega)$ spectra due to photocarriers. From the analyses of $\tilde{\sigma}(\omega)$ spectra with a two-carrier Drude model, we evaluated the electron-hole scattering rate $\gamma_{\text{e-h}}$ at various temperatures and photocarrier densities. By comparing the temperature dependence of $\gamma_{\text{e-h}}$ with that deduced from a theoretical model including the effects of Rutherford scatterings, the screening of Coulomb interactions, and Pauli exclusion [9–12], we discuss the mechanism of electron-hole scatterings in silicon.

As a sample, we used a nondoped silicon single crystal with the thickness of 1 mm, whose resistivity is larger than 1000 Ω cm at 293 K. For optical-pump terahertz-probe spectroscopy, we utilized as the light source a Ti:sapphire regenerative amplifier with a pulse energy of 2.4 mJ, a central photon energy of 1.55 eV, a pulse duration of 25 fs, and a repetition rate of 1 kHz. The output from the amplifier was divided into two beams. One was used for the generation of pump pulses (1.77–2.53 eV) using an optical parametric amplifier. The other was used for the generation and detection of THz probe pulses. We employed air-plasma-induced terahertz radiation in order to obtain broadband (0.8–7.2 THz) pulses [15,16]. Temporal wave forms of THz probe pulses transmitted through the sample were measured by electro-optical (EO) sampling with a 300-μm-thick GaP crystal, in which the detectable probe range is 0.8-7.2 THz. In order to obtain $\tilde{\sigma}(\omega)$ spectra, we alternately measured wave forms of transmitted THz pulses without a pump pulse $E(t)$ [Fig. 1(b)] and with a pump pulse $E(t) + \Delta E(t)$ [Fig. 1(c)] by using two optical choppers. We extracted $\tilde{\sigma}(\omega)$ using the following equation [17–19],

$$\tilde{\sigma}(\omega) = -\frac{\epsilon_0 c\,(n_0 + 1)}{L}\frac{\Delta\tilde{E}(\omega)}{\tilde{E}(\omega)}, \tag{1}$$

where ϵ_0 is the vacuum permittivity, c the velocity of light, n_0 the refractive index of silicon in the terahertz frequency region ($n_0 = 3.4$), and L the penetration depth of pump pulses. L is obtained from the absorption-coefficient (α) spectra [20,21]. $\tilde{E}(\omega)$ and $\Delta\tilde{E}(\omega)$ are complex Fourier transforms of $E(t)$ and $\Delta E(t)$, respectively. Typical wave forms of $E(t)$ and $E(t) + \Delta E(t)$ and their relative Fourier components [$|\Delta\tilde{E}(\omega)/\tilde{E}(\omega)|$ and $\Delta\phi(\omega)$] are presented in Figs. 1(d) and 1(e), respectively. The delay time t_d of a THz probe pulse [the maximum of $|E(t)|$] relative to a pump pulse was adjusted by changing the path length of the pump pulse.

Figure 2(a) shows $\tilde{\sigma}(\omega)$ spectra at 293 K, which were obtained by a 1.77 eV pump (the excitation density $x_{\text{ph}} = 1.3 \times 10^2\ \mu\text{J/cm}^2$ [22]) at $t_d = 2$ ps, when a pump pulse and a THz pulse are completely separated in the time domain. To

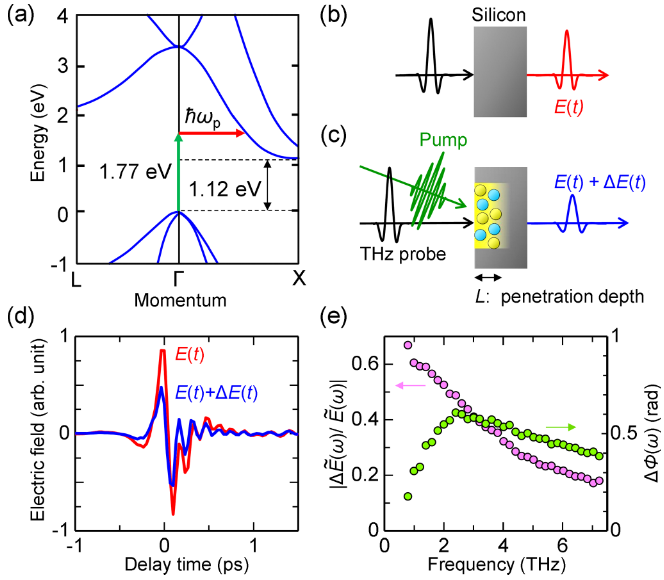

FIG. 1. (Color online) (a) Band structure of silicon [14]. (b), (c) Schematics of optical-pump terahertz-probe spectroscopy (b) without and (c) with a pump pulse. (d) Terahertz electric-field wave forms with $[E(t)+\Delta E(t)]$ and without $[E(t)]$ a pump pulse. (e) Transient complex transmissivity $[|\Delta\tilde{E}(\omega)/\tilde{E}(\omega)|$ and $\Delta\phi(\omega)]$ spectra due to photocarriers.

analyze $\tilde{\sigma}(\omega)$ spectra, we adopt a two-carrier Drude model,

$$\tilde{\sigma}(\omega) = ne^2\left(\frac{1}{m_e}\frac{1}{\gamma_e - i\omega} + \frac{1}{m_h}\frac{1}{\gamma_h - i\omega}\right), \qquad (2)$$

where n is carrier density of the electron or hole, m_e (m_h) is the effective mass of the electron (hole), and γ_e (γ_h) is the scattering rate of the electron (hole). γ_e (γ_h) is the sum of an electron-hole scattering and a carrier-phonon scattering according to the Mathiesen's law, $\gamma_e = \gamma_{e\text{-}h} + \gamma_{e\text{-}p}$ $(\gamma_h = \gamma_{e\text{-}h} + \gamma_{h\text{-}p})$, where $\gamma_{e\text{-}p}$ $(\gamma_{h\text{-}p})$ is an electron (hole)-phonon scattering rate. From mobility values of chemically doped silicon with low carrier concentrations of 1.0×10^{14} cm^{-3} for an electron and 1.0×10^{15} cm^{-3} for a hole at room temperature [8], we deduced $\gamma_{e\text{-}p}$ and $\gamma_{h\text{-}p}$ using the general formula $\mu = e/m^*\gamma$. For the effective masses, we used literature values, $m_e = 0.26m_0$ and $m_h = 0.37m_0$ (m_0 is the free electron mass) [23]. Thus, we fit Eq. (2) to the experimental $\tilde{\sigma}(\omega)$ data with two fitting parameters, n and $\gamma_{e\text{-}h}$. We neglected scatterings between the same kinds of carriers (electron-electron and hole-hole scatterings). These scatterings do not contribute to the relaxation of currents, because the momentum is conserved during the scattering processes [12,13]. In Fig. 2(a), dashed lines are fitted curves with $\gamma_{e\text{-}h}/2\pi = 3.9$ THz and $n = 2.6 \times 10^{17}$ cm^{-3}, which reproduce well the $\tilde{\sigma}(\omega)$ spectra. The responses of electrons and holes are shown by different colors. From the values of $\gamma_{e\text{-}h}$, the mobilities of the electrons and holes are deduced to be $\mu_e = e/m_e\gamma_e = 2.3 \times 10^2$ cm^2/V s and $\mu_h = e/m_h\gamma_h = 1.4 \times 10^2$ cm^2/V s, respectively.

In the analyses presented above, we did not take into account the spatial diffusions of photocarriers, which should give rise to errors in the evaluated values of n and $\gamma_{e\text{-}h}$. To investigate the carrier diffusion effects, we measured the excitation-photon-energy (E_{ex}) dependence of $\gamma_{e\text{-}h}$ at 293 K

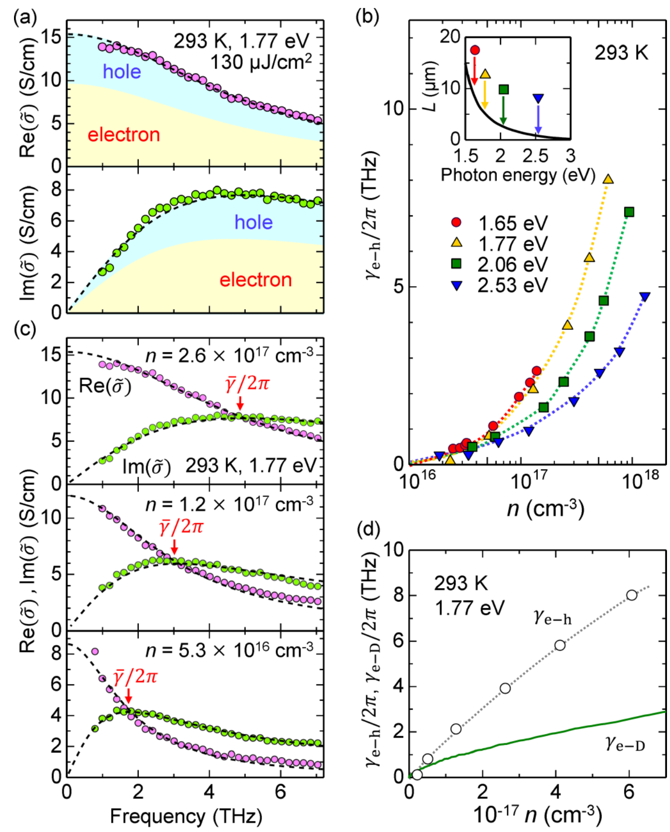

FIG. 2. (Color online) (a) $\mathrm{Re}(\tilde{\sigma})$ and $\mathrm{Im}(\tilde{\sigma})$ spectra in silicon measured with a 1.77 eV pump at 293 K. Dashed lines indicate fitting curves. The responses of electrons and holes are shown by shades. (b) Carrier-density dependence of $\gamma_{e\text{-}h}$. Penetration depth for each pump energy is shown in the inset [20]. (c) $\mathrm{Re}(\tilde{\sigma})$ and $\mathrm{Im}(\tilde{\sigma})$ spectra for different pump photon densities. Crossing points correspond to $\bar{\gamma}/2\pi$. Dashed lines are fitting curves. (d) Carrier-density dependence of $\gamma_{e\text{-}h}$. Electron-ionized-impurity scattering $\gamma_{e\text{-}D}$ in n-type silicon is shown by the solid line [8].

and $t_d = 2$ ps, which is shown in Fig. 2(b). $\gamma_{e\text{-}h}$ changes depending on E_{ex}, which is attributable to the presence of carrier diffusions. With an increase of E_{ex}, L becomes shorter [the inset of Fig. 2(b)] [20], leading to the enhancement of carrier diffusion effects. However, the 1.65 and 1.77 eV excitations give the same $\gamma_{e\text{-}h}$ values at the same n values, so that carrier diffusions can be neglected for these energies at $t_d = 2$ ps. Thus, we selected $E_{ex} = 1.77$ eV and $t_d = 2$ ps for the measurements of $\tilde{\sigma}(\omega)$ [24].

Next, we discuss the carrier-density dependence of $\tilde{\sigma}(\omega)$ in more detail. Figure 2(c) shows $\tilde{\sigma}(\omega)$ spectra at $t_d = 2$ ps for three carrier densities, $n = 2.6 \times 10^{17}$, 1.3×10^{17}, and 5.2×10^{16} cm^{-3}. With an increase of the carrier density, the crossing point of the real and imaginary parts which corresponds to the average carrier scattering rate $\bar{\gamma}/2\pi$ shifts to a higher energy. Figure 2(d) shows the carrier-density dependence of $\gamma_{e\text{-}h}$. In the low carrier-density region, $\gamma_{e\text{-}h}$ increases linearly with carrier density, reflecting the increase in the encounter rate of an electron and a hole. This trend is consistent with the previous result reported by Hendry *et al.* [13]. In the high carrier-density region, $\gamma_{e\text{-}h}$ deviates from the linear dependence and tends to saturate, which is attributable to the screening of

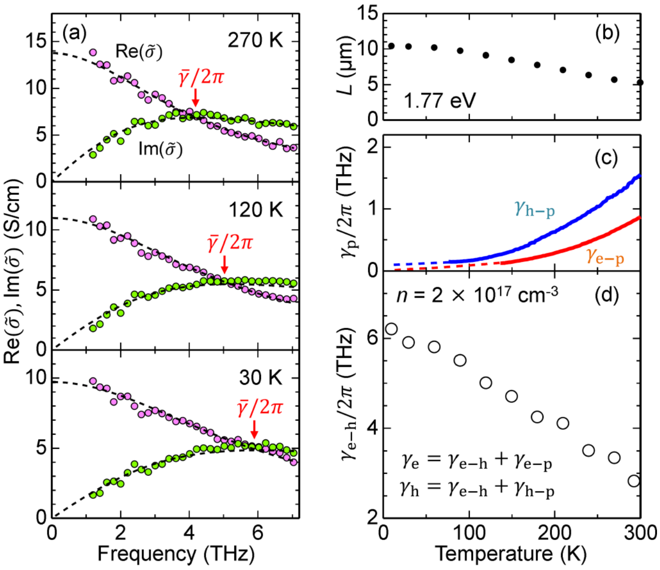

FIG. 3. (Color online) (a) Temperature dependence of $\tilde{\sigma}(\omega)$ for the 1.77 eV pump ($n = 2.0 \times 10^{17}$ cm^{-3}). Dashed lines indicate fitting curves. (b) Temperature dependence of the penetration depth L at 1.77 eV [21]. (c) Temperature dependence of $\gamma_{\text{e-p}}$ and $\gamma_{\text{h-p}}$ (see text) [26,27]. Dashed lines are extrapolated curves. (d) Temperature dependence of $\gamma_{\text{e-h}}$.

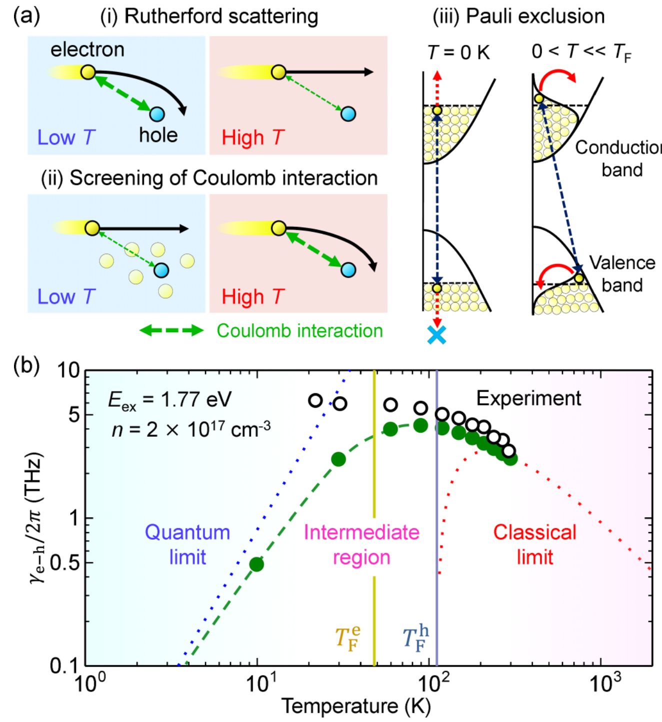

FIG. 4. (Color online) (a) Schematics of (i) Rutherford scatterings, (ii) screening of Coulomb interactions at low temperatures (low T) and high temperatures (high T), and (iii) Pauli exclusion at $T = 0$ K and $0 < T \ll T_F$. At $T = 0$ K, electron-hole scatterings are prohibited. (b) Open circles show the temperature dependence of $\gamma_{\text{e-h}}$ shown in Fig. 3(d). Solid circles show theoretical values obtained from Eqs. (6) and (7). Values in classical and quantum limits are also shown by dotted lines.

the Coulomb interaction between the electron and hole due to other carriers. Such a behavior is consistent with the theory reported by Combescot *et al.* [9,10]. The electron-density (i.e., dopant-density) dependence of the electron-ionized-impurity scattering rate $\gamma_{\text{e-D}}$ in phosphorus-doped n-type silicon is also shown by a solid line in Fig. 2(d) [8]. $\gamma_{\text{e-D}}$ is smaller than a half of $\gamma_{\text{e-h}}$. In the case of chemically doped samples, ionized impurities are fixed at lattice points and cannot move around. This causes a decrease in the encounter rate between the electron (hole) and donor (acceptor) compared to the case of photogenerated electrons and holes, both of which are mobile. Thus, the scattering rate between the electron (hole) and donor (acceptor) is smaller than that between photogenerated electrons and holes. As a result, at the same carrier density, the mobilities of the photocarriers become smaller than those of carriers injected by elemental substitutions [25].

To investigate the mechanism for electron-hole scatterings, which is the main subject of the present study, we measured the temperature dependence of $\gamma_{\text{e-h}}$. In this experiment, we adjusted x_{ph} so that the carrier density was constant ($n = 2.0 \times 10^{17}$ cm^{-3}) at all temperatures, taking into account the temperature dependence of the penetration depth L [Fig. 3(b)] [21]. Figure 3(a) shows $\tilde{\sigma}(\omega)$ spectra at three typical temperatures, 270, 120, and 30 K. $\bar{\gamma}/2\pi$ increases with decreasing temperature. To determine $\gamma_{\text{e-h}}$, we calculated $\gamma_{\text{e-p}}$ and $\gamma_{\text{h-p}}$ using the temperature dependence of the mobilities in n-type silicon with a dopant density of 1.2×10^{14} cm^{-3} [26] and in p-type silicon with a dopant density of 4.5×10^{14} cm^{-3} [27], which are shown in Fig. 3(c). The dashed lines are freehand extrapolations. The error of the extrapolation does not affect the analysis because $\gamma_{\text{e-p}}$ and $\gamma_{\text{h-p}}$ are almost equal to zero in this temperature region. Using these values, we obtained the temperature dependence of $\gamma_{\text{e-h}}$ [Fig. 3(d)], which increases monotonically as the temperature decreases.

To interpret the temperature (T) dependence of $\gamma_{\text{e-h}}$, we refer to the theoretical study reported by Combescot *et al.*, in which the scattering mechanism was discussed in two limiting cases: $T \gg T_F$ (classical limit) and $T \ll T_F$ (quantum limit). Here, T_F is the Fermi temperature [$T_F = \hbar^2/2mk_B(\frac{3\pi^2 n}{6})^{2/3}$], where $\hbar$ is the reduced Planck constant and k_B is the Boltzmann constant. In the classical limit, the carriers are regarded as classical particles and $\gamma_{\text{e-h}}$ is dominated by Rutherford scatterings caused by Coulomb interactions and the screening of Coulomb interactions. The Rutherford scattering is a general mechanism of the scattering between charged particles, which is proportional to $T^{-3/2}$ [9]. With decreasing temperature, a particle is easily captured by an oppositely charged carrier due to the reduction of its velocity [Fig. 4(a)(i)], so that $\gamma_{\text{e-h}}$ increases. At low temperatures, however, the screening effect is enhanced by carrier-velocity reductions and rather suppresses $\gamma_{\text{e-h}}$ as $\gamma_{\text{e-h}} \propto \ln T$ [Fig. 4(a)(ii)]. Taking these two mechanisms into account, the temperature dependence of $\gamma_{\text{e-h}}$ can be calculated by the Boltzmann approach [9,10] as

$$\gamma_{\text{e-h}} = \frac{16}{9\pi^{3/2}} k_B T_{\text{Ryd}} \left(\frac{T_F}{T}\right)^{3/2} \ln\left(\frac{T^2}{T_{\text{Ryd}}^{1/2} T_F^{3/2}}\right). \tag{3}$$

Here, $k_B T_{\rm Ryd}(=me^4/2\hbar^2\epsilon^2)$ corresponds to the exciton binding energy, which scales the Coulomb interaction between an electron and a hole. $m = (\frac{1}{m_e} + \frac{1}{m_h})^{-1}$ and ϵ is the static permittivity of silicon. The calculated curve in our experimental condition [Fig. 3(d)] is shown by the red dotted line in Fig. 4(b) [28].

In the quantum limit ($T \ll T_F$), carriers degenerate into the bottom of the band (Fermi degeneracy). Due to the energy conservation law, the interaction between an electron and a hole is reduced and $\gamma_{\text{e-h}}$ goes to zero at $T = 0$ K [Fig. 4(a)(iii)]. For $0 < T \ll T_F$, carriers around the Fermi surface can be excited and scatter each other. The number of these carriers is proportional to T, so that $\gamma_{\text{e-h}} \propto T^2$ [Fig. 4(a)(iii)]. As a result, $\gamma_{\text{e-h}}$ is written by the following equation [11],

$$\gamma_{\text{e-h}} = \frac{1}{6}k_B T_{\rm Ryd}\left(\frac{T}{T_F}\right)^2\left(x\tan^{-1}x - \frac{x^2}{1+x^2}\right)\pi\nu^{4/3}\left(\frac{m_e^2 m_h^2}{m^4}\right), \tag{4}$$

$$x = \frac{\nu^{1/6}\pi^{1/2}m^{1/2}}{(\nu m_e + \nu^{1/3}m_h)^{1/2}}\left(\frac{T_F}{T_{\rm Ryd}}\right)^{1/4}, \tag{5}$$

where ν is the conduction-band degeneracy and is equal to 6 in silicon [8]. The temperature dependence of $\gamma_{\text{e-h}}$ calculated by Eq. (4) for $0 < T \ll T_F$ is denoted by the blue dotted line in Fig. 4(b).

Around $T \sim T_F$, both classical and quantum effects should be considered. Sernelius calculated $\gamma_{\text{e-h}}$ in this intermediate region by utilizing the generalized Drude model and Kubo formula [11,12,29]. According to his calculation,

$$\sigma(0) = \frac{e^2}{\eta_{\text{e-h}}} = \frac{ne^2}{m\gamma_{\text{e-h}}}, \tag{6}$$

$$\eta_{\text{e-h}} = \frac{6\hbar^2\beta}{n^2}\int_0^\infty \frac{d\omega}{2\pi}\frac{1}{\sinh^2\frac{\hbar\beta\omega}{2}} \times \int \frac{d\boldsymbol{q}}{(2\pi)^3}q_u^2 \frac{\mathrm{Im}\alpha_e(\boldsymbol{q},\omega)\mathrm{Im}\alpha_h(\boldsymbol{q},\omega)}{|1+6\alpha_e(\boldsymbol{q},\omega)+\alpha_h(\boldsymbol{q},\omega)|^2}, \tag{7}$$

where $\beta = 1/k_B T$ and α_e (α_h) is the polarizability of electron (hole) obtained by a random phase approximation [30]. $\boldsymbol{q}$ and q_u are the momentum and its projection on the direction of the electric field, respectively. Only the imaginary part of the polarizability can be obtained analytically, so that we calculated the real part with the use of the Kramers-Kronig relation and obtained the temperature dependence of $\gamma_{\text{e-h}}$ from Eqs. (6) and (7) for our experimental condition ($n = 2.0 \times 10^{17}$ cm^{-3}), which is shown by solid circles in Fig. 4(b). This curve has a peak at around $T \sim T_F$ and coincides with the curves of classical and quantum limits for $T \gg T_F^h$ (the Fermi temperature of holes) and $T \ll T_F^e$ (the Fermi temperature of electrons), respectively [31].

In Fig. 4(b), we showed again the experimental $\gamma_{\text{e-h}}$ data of Fig. 3(d) by open circles. For $T \gg T_F^h$, the absolute values of $\gamma_{\text{e-h}}$ as well as their temperature dependence are well reproduced by the theoretical curve. This demonstrates that electron-hole scattering is explained by the above-mentioned three mechanisms. Below 60 K, the theoretical curve turns downward, reflecting the quantum effect, but the experimental $\gamma_{\text{e-h}}$ does not show such a decrease.

A possible origin for the deviation of the experimental $\gamma_{\text{e-h}}$ from the theoretical one is an excess energy of the photocarriers, since $E_{\rm ex}$(1.77 eV) was 0.65 eV larger than the indirect gap of silicon (1.12 eV) [Fig. 1(a)]. The previous two-photon photoemission spectroscopy revealed that at 296 and 90 K, photocarriers are rapidly relaxed and thermally equilibrated to phonons at $t_d = 2$ ps [32,33]. Judging from these results, we can consider that the increase of temperature at that time is very small (<5 K) above 90 K. This is the reason why the $\gamma_{\text{e-h}}$ values evaluated at $t_d = 2$ ps are in accord with the theoretical values at $T \gg T_F^h$.

On the other hand, it was suggested from optical-pump terahertz-probe spectroscopy that it takes several hundred picoseconds for the carriers to relax below 60 K [5]. Such a long relaxation time is attributable to small populations of phonons. Therefore, it is reasonable to consider that below 60 K, photocarriers at $t_d = 2$ ps have finite kinetic energies or equivalently high temperatures. This would be the reason why the experimental data are larger than theoretical ones.

In summary, we measured optical conductivity $\tilde{\sigma}(\omega)$ spectra due to photocarriers in nondoped silicon by optical-pump terahertz-probe spectroscopy. By analyzing $\tilde{\sigma}(\omega)$ spectra with the two-carrier Drude model, electron-hole scattering rates $\gamma_{\text{e-h}}$ were evaluated. From 293 to 90 K, the absolute values and temperature dependence of $\gamma_{\text{e-h}}$ were well reproduced by the theoretical curve, in which Rutherford scattering, Coulomb screening, and Pauli exclusion were taken into account. This demonstrates that these three factors can explain electron-hole scattering processes in silicon.

We thank Professor B. E. Sernelius (Linköping University) for a private communication regarding a calculation procedure of the electron-hole scattering rate, and Professor R. Shimano (University of Tokyo) for providing thin single crystals for the measurements of the temperature dependence of the absorption coefficient. T.T. was supported by JSPS through the Program for Leading Graduate Schools (MERIT). This work was partly supported by a Grant-in-Aid for Scientific Research from JSPS (No. 22740197).

[1] S. W. Koch, W. Hoyer, M. Kira, and V. S. Filiov, Phys. Status Solidi B **238**, 404 (2003).

[2] D. Semkat, F. Richter, D. Kremp, G. Manzke, W.-D. Kraeft, and K. Henneberger, Phys. Rev. B **80**, 155201 (2009).

[3] T. Suzuki and R. Shimano, Phys. Rev. Lett. **103**, 057401 (2009).

[4] R. Shimano and T. Suzuki, Phys. Status Solidi C **8**, 1153 (2011).

[5] T. Suzuki and R. Shimano, Phys. Rev. B **83**, 085207 (2011).

[6] R. A. Kaindl, M. A. Carnahan, D. Hägele, R. Lövenich, and D. S. Chemla, Nature (London) **423**, 734 (2003).

[7] R. A. Kaindl, D. Hägele, M. A. Carnahan, and D. S. Chemla, Phys. Rev. B **79**, 045320 (2009).
[8] S. M. Sze, *Semiconductor Devices: Physics and Technology*, 2nd ed. (Wiley, New York, 1986).
[9] M. Combescot and R. Combescot, Phys. Rev. B **35**, 7986 (1987).
[10] M. Combescot, Solid-State Electron. **31**, 657 (1988).
[11] B. E. Sernelius, Phys. Rev. B **40**, 12438 (1989).
[12] B. E. Sernelius, Phys. Rev. B **43**, 7136 (1991).
[13] E. Hendry, M. Koeberg, J. Pijpers, and M. Bonn, Phys. Rev. B **75**, 233202 (2007).
[14] J. R. Chelikowsky and M. L. Cohen, Phys. Rev. B **10**, 5095 (1974).
[15] D. J. Cook and R. M. Hochstrasser, Opt. Lett. **25**, 1210 (2000).
[16] H. G. Roskos, M. D. Thomson, M. Kreß, and T. Löffler, Laser Photonics Rev. **1**, 349 (2007).
[17] H.-K Nienhuys and V. Sundstrom, Phys. Rev. B **71**, 235110 (2005).
[18] Equation (1) is deduced by the two-layer model, in which photocarriers are distributed homogeneously within the penetration depth of the pump light. In order to check the validity of the two-layer model, we calculated the spectrum of photoinduced absorption changes using the multilayer model, in which the exponential-type photocarrier distribution is taken into account [19]. The spectra obtained by those two models are essentially the same, supporting the validity of the two-layer model.
[19] H. Matsuzaki, Y. Matsui, R. Uchida, H. Yada, T. Terashige, B.-S. Li, A. Sawa, M. Kawasaki, Y. Tokura, and H. Okamoto, J. Appl. Phys. **115**, 053514 (2014).
[20] M. A. Green and M. J. Keevers, Progr. Photovoltaics **3**, 189 (1995).
[21] We obtained the temperature dependence of the absorption coefficient in the visible region by transmittance and reflectivity measurements of a thin silicon single crystal (20 μm).
[22] The energy profile $W(x,y)$ of the pump pulse is of the Gaussian type, $W(x,y) \propto \exp(-\frac{x^2+y^2}{r^2})$. Here, $2r$ is the diameter of the pump pulse, which is 2 mm in this study. The sample is attached to a pinhole with a diameter of 1 mm. x_{ph} was evaluated by the equation $x_{\mathrm{ph}} = \frac{I_0}{\pi r^2}$, where I_0 is the energy of the pump pulse.
[23] M. A. Green, J. Appl. Phys. **67**, 2944 (1990).
[24] When we use a thin single crystal with a thickness comparable to the absorption depth of the pump light to avoid a diffusion effect, multiple reflections within the crystal will occur, which makes it difficult to analyze transmitted THz waves.
[25] For example, at $n = 2.6 \times 10^{17}\ \mathrm{cm}^{-3}$, the mobilities of photocarriers ($\mu_{\mathrm{e}} = 2.3 \times 10^2\ \mathrm{cm}^2/\mathrm{V\,s}$ and $\mu_{\mathrm{h}} = 1.4 \times 10^2\ \mathrm{cm}^2/\mathrm{V\,s}$) are smaller than those of chemically doped carriers ($\mu_{\mathrm{e}} = 4.9 \times 10^2\ \mathrm{cm}^2/\mathrm{V\,s}$ and $\mu_{\mathrm{h}} = 2.4 \times 10^2\ \mathrm{cm}^2/\mathrm{V\,s}$) [8]. This is due to large $\gamma_{\text{e-h}}$ values compared to $\gamma_{\text{e-D}}$ and $\gamma_{\text{h-A}}$ (hole-acceptor scattering).
[26] S. S. Li and W. Robert Thurber, Solid-State Electron. **20**, 609 (1977).
[27] S. S. Li, Solid-State Electron. **21**, 1109 (1978).
[28] Equation (3) is valid only for $T \gg T_{\mathrm{F}}$ and a singularity at $T \sim T_{\mathrm{F}}$ in Fig. 4(b) is an artifact due to the approximation used in the derivation of Eq. (3) [9].
[29] B. E. Sernelius, J. Phys.: Condens. Matter **3**, 1493 (1991).
[30] The derivation of Eq. (7) is described in Ref. [12]. Equation (12) of Ref. [29] was used for the calculation of α_{e} and α_{h} in Eq. (7).
[31] In the calculation of Eq. (7), we have to consider $T_{\mathrm{F}}^{\mathrm{e}}$ and $T_{\mathrm{F}}^{\mathrm{h}}$ instead of T_{F} [12].
[32] T. Ichibayashi and K. Tanimura, Phys. Rev. Lett. **102**, 087403 (2009).
[33] T. Ichibayashi, S. Tanaka, J. Kanasaki, K. Tanimura, and T. Fauster, Phys. Rev. B **84**, 235210 (2011).